ISSN 1087-6596, Glass Physics and Chemistry, 2023, Vol. 49, No. 6, pp. 657–663. © Pleiades Publishing, Ltd., 2023.
Russian Text © The Author(s), 2023, published in Fizika i Khimiya Stekla.

Synthesis and Structure of New Potassium and Cesium Zinc Diphosphates

D. I. Tsygankova[a, b], O. Yu. Sinel'shchikova[a, *], and V. L. Ugolkov[a]

[a] *Grebenshchikov Institute of Silicate Chemistry, Russian Academy of Sciences, St. Petersburg, 199034 Russia*
[b] *Ulyanov (Lenin) St. Petersburg State Electrotechnical University "LETI," St. Petersburg, 197022 Russia*
**e-mail: sinelshikova@mail.com*

Received May 29, 2023; revised August 1, 2023; accepted August 7, 2023

Abstract—This article presents the results of a study of new solid solutions formed in the system of diphosphates of alkaline elements and zinc: $K_2Zn_3(P_2O_7)_2$–$Cs_2Zn_3(P_2O_7)_2$. The obtained materials are promising as matrices for creating phosphors. The formation of phases containing two alkali cations is established on samples obtained by solid-phase synthesis by X-ray phase analysis, and the results of studying their thermal stability are presented.

Keywords: solid-phase synthesis, alkali metal diphosphates, solid solutions
DOI: 10.1134/S1087659623600643

INTRODUCTION

Complex diphosphates of alkali metals are of practical interest as ionic conductors [1–3], ferroelectric and piezoelectric materials [4, 5], and the base for obtaining glasses, including luminescent ones [4, 6–14]. For crystalline materials, one of the most interesting areas of application is the creation of phosphors based on them, which are applicable, among other things, for manufacturing light-emitting diodes, and optical materials that are transparent in the UV range [15–22]. The most interesting diphosphates are compounds exhibiting nonlinear optical properties; and examples of such phases are $RbNaMgP_2O_7$ [23], $Rb_2Ba_3(P_2O_7)_2$ [24], α-$Rb_2Mg_3(P_2O_7)_2$ [25], $Rb_2Zn_3(P_2O_7)_2$ [26], $K_4Mg_4(P_2O_7)_3$ and $Rb_4Mg_4(P_2O_7)$ [27].

Diphosphates are often characterized by a fairly flexible structure due to the change in the orientation of the P_2O_7 dimers, which leads to the frequent manifestation of polymorphism and wide isomorphic substitutions in the crystal lattice [28, 29]. In the stoichiometry of $M_2ZnP_2O_7$, where M are alkali metals, the existence of solid solutions and compounds containing up to three different monovalent cations was confirmed [1, 29–31].

In the stoichiometry of $M_2Zn_3(P_2O_7)_2$, the following groups crystallizing in noncentrosymmetric space groups are known: $K_2Zn_3(P_2O_7)_2$, sp. group $P2_12_12_1$ [32]; and $Rb_2Zn_3(P_2O_7)_2$, sp. group $P2_1$ [6]; and $Cs_2Zn_3(P_2O_7)_2$ [26], which has the centrosymmetric sp. group $P2_1/c$. Solid solutions crystallizing in the stoichiometry of $M_2Zn_3(P_2O_7)_2$ and containing two alkali metals were not previously considered; therefore, studying the phase formation in the $K_2Zn_3(P_2O_7)_2$–$Cs_2Zn_3(P_2O_7)_2$ system is an urgent task, and it will give a new insight into the development of diphosphates based on directed isomorphic substitutions.

EXPERIMENTAL

Polycrystalline samples were synthesized in the studied system by the method of solid-phase reactions. For this, the initial KPO_3, Cs_2CO_3, ZnO (chemically pure grade), and $NH_4H_2PO_4$ (special-purity grade) reagents were taken in ratios corresponding to the stoichiometry of the extreme members of the system under consideration: $K_2Zn_3(P_2O_7)_2$ and $Cs_2Zn_3(P_2O_7)_2$ were crushed and homogenized in a planetary mill (Pulverizette 6) for 0.5 h at a speed of 350 rpm. The powders thus obtained were pressed into tablets 10 mm in diameter with a force of 4 tons. Potassium and cesium zinc phosphate were fired in porcelain crucibles in two stages. The first one was at 550°C and the second one was for $K_2Zn_3(P_2O_7)_2$ at 730°C and for $Cs_2Zn_3(P_2O_7)_2$ at 650°C. The holding time at each stage was 18 h; between the stages, the samples were subjected to intermediate grinding and repeated pressing.

The compositions thus obtained were crushed and used as the starting materials for the synthesis of samples corresponding to the stoichiometry of $K_{2-x}Cs_xZn_3(P_2O_7)_2$

Table 1. Unit cell parameters of synthesized solid solutions in comparison with known compounds of the same stoichiometry

Chemical formula	x	Sp. gr.	a, Å	b, Å	c, Å	β, deg	V, Å^3
$K_2Zn_3(P_2O_7)_2$*	0.0	$P2_12_12_1$	12.901(8)	10.102(6)	9.958(1)	90	1297.955(9)
$K_{2-x}Cs_xZn_3(P_2O_7)_2$ Phase I	0.4	$P2_1$	7.1164(10)	7.1459(9)	13.0773(15)	91.37(1)	664.82(11)
	0.5		7.1292(8)	7.1622(11)	13.0793(15)	91.34(1)	667.66(11)
	0.6		7.1335(9)	7.1675(11)	13.0831(17)	91.55(1)	668.68(11)
$K_{2-x}Cs_xZn_3(P_2O_7)_2$ Phase II	1.4	$P2_1/c$	13.3297(26)	7.3605(10)	14.4952(17)	90.89(1)	1422.01(28)
	1.6		13.3869(20)	7.3608(09)	14.5151(17)	90.96(1)	1430.09(24)
	1.8		13.4040(22)	7.3756(10)	14.5495(18)	91.04(1)	1438.16(26)
$Cs_2Zn_3(P_2O_7)_2$*	2.0		13.453(5)	7.407(3)	14.603(5)	91.203(5)	1454.9(9)
$Rb_2Zn_3(P_2O_7)_2$*	–	$P2_1$	7.1950(3)	7.2206(3)	13.2128(5)	92.1120(1)	685.97(5)

* Published data [26, 32].

at $x = 0.2$–1.8 with a step of 0.2. Powders of complex oxides taken in molar ratios were mixed by hand in an agate mortar for 15 min, after which they were pressed, similarly to the initial compositions, and fired at 650°C with exposure ranging from 5 to 18 h.

The phase composition of the samples at different stages of firing was determined using X-ray phase analysis (XPA). The surveys were carried out on a DRON-3M diffractometer (radiation of CuK_α) at room temperature in the range of Bragg angles of 2θ of 10°–70° in steps of 0.02 deg.

The thermal behavior of the synthesized samples was studied on an STA 429 thermal analyzer (Netzsch) in the temperature range 25–1000°C. The sample weight was 30–100 mg. The survey was carried out using platinum crucibles in the heating mode at a rate of 10 deg/min. The onset of the thermal effect was determined by the intersection of the tangents to the baseline of the differential scanning calorimetry (DSC) curves and to the initial branch of the thermal effect curve.

The IR spectra of the obtained compositions were measured on an Infraspec FSM 2202 instrument in the wavenumber range from 4000 to 400 cm^{-1} at room temperature. KBr served as the standard of comparison; its mixture with the studied composition was placed in a mold from which air was pumped out for 10 min, and then pressed into tablets with a diameter of 12 mm.

RESULTS AND DISCUSSION

The results of the X-ray phase analysis of the synthesized samples are shown in Fig. 1.

As can be seen from the diffraction patterns, the sample at $x = 0.0$ corresponds to single-phase $K_2Zn_3(P_2O_7)_2$, and the samples with a cesium content of $x = 0.4$–0.6 represent a limited solid solution (hereinafter, phase I), which can be identified in the space group $P2_1$. This structure was previously found in the $Rb_2Zn_3(P_2O_7)_2$ compound [26]. It is characterized by the presence of endless tunnels in the zinc-phosphate framework filled with alkali metal atoms. The central part of the diffraction pattern of one of the compositions of phase I in comparison with the theoretical diffraction pattern of isostructural rubidium-zinc diphosphate is shown in Fig. 2. The potassium and cesium in the resulting solid solution, probably similarly to the rubidium analog, are coordinated by nine oxygen atoms. It is interesting to note that KO_8 polyhedra are realized in $K_2Zn_3(P_2O_7)_2$; and CsOn ($n = 9, 12$), in $Cs_2Zn_3(P_2O_7)_2$. The average crystal radius according to Shannon for alkali cations in the realized coordination for the obtained solid solution is R_K = 1.60...1.64 Å, which is close to the size of rubidium ions (R_K = 1.69 Å). A more detailed description of the crystal structures with visualization of these polyhedra and the crystal structure of the framework for the considered phases is given in [26, 32].

The sample at $x = 0.2$ is two-phase, and it contains potassium zinc phosphate and phase I. At $x \geq 1.4$ a solid solution $K_{2-x}Cs_xZn_3(P_2O_7)_2$ is formed based on the $Cs_2Zn_3(P_2O_7)_2$ compound, which possesses the space group $P2_1/c$ (further, phase II). Two-phase compositions, containing a mixture of phases I and II, are compositions that lie in the concentration range from $x = 0.8$ to 1.2.

The unit cell parameters of phases I and II obtained in this study, calculated using the least squares method, as well as individual compounds indicated according to the published data, are given in Table 1. An increase in the cesium content is accompanied by

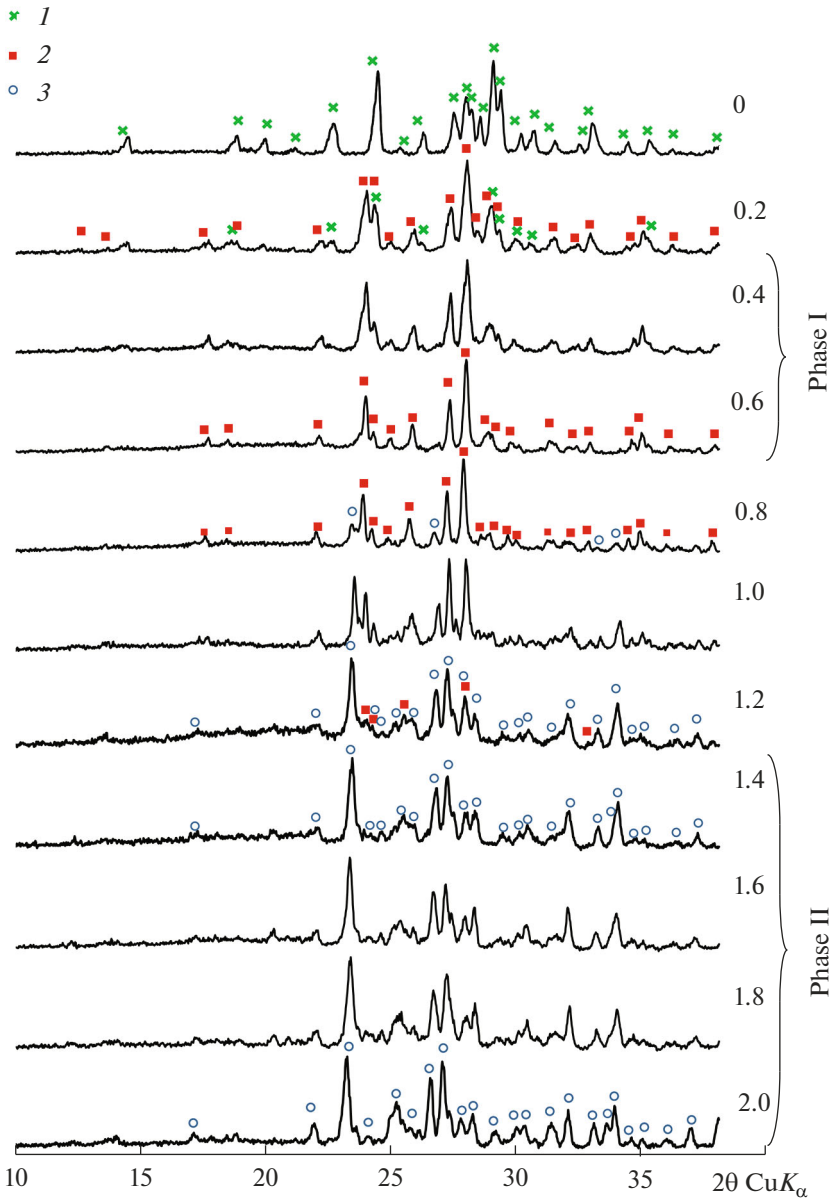

Fig. 1. X-ray diffraction patterns of samples of $K_{2-x}Cs_xZn_3(P_2O_7)_2$ composition, at different cesium content (x indicated in the figure). Symbols for reflexes: (*1*) $K_2Zn_3(P_2O_7)_2$; (*2*) phase I; (*3*) phase II.

an increase in the size of the crystal cell; however, for the extreme composition of the phase I solid solution at $x = 0.6$, it remains smaller than that of the rubidium analog (see Table 1).

Based on the data obtained, it can be concluded that the volume occupied by the formula unit (Fig. 3) increases with the increase in the cesium content, which is true for all three structures implemented in the section. This result is in close agreement with the increase in the average ionic radius of the alkali metal.

The "fingerprint" region of the IR spectra of a number of obtained samples, including the crystallization region of phase I, is shown in Fig. 4. The absorption peaks with the maxima lying at 1210–1110 cm^{-1} are asymmetric; and those with maxima at 975–950 cm^{-1} are symmetric P–O stretching vibrations in PO_4 tetrahedra. The absorption band around 735–765 cm^{-1} can be attributed to the stretching vibrations of the P–O–P bridges. In addition, the absorption peaks in the range from 645 to 527 cm^{-1} can be attributed to the asymmetric O–P–O bending vibrations and symmetric O–P–O bending vibrations in PO_4, respectively [26, 27]. The presence of all the reflections

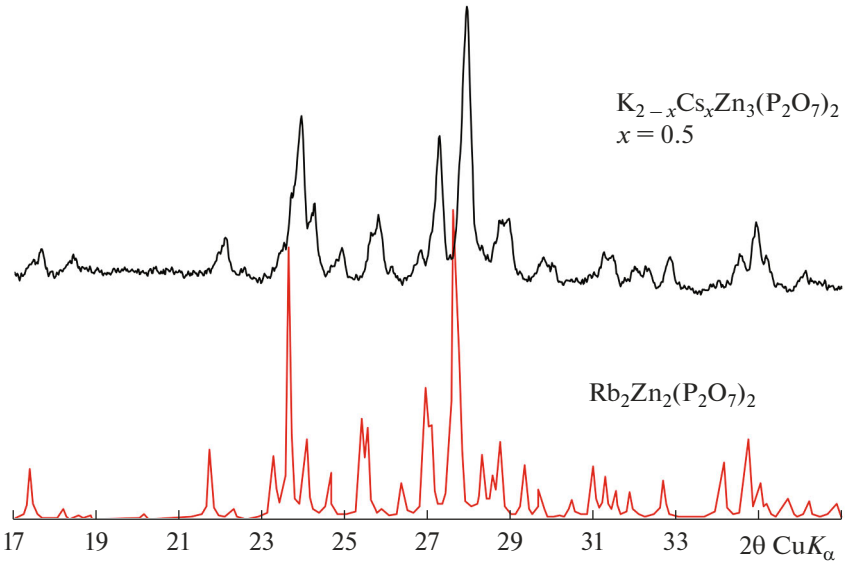

Fig. 2. Experimental diffraction pattern of a sample of composition $K_{2-x}Cs_xZn_3(P_2O_7)_2$ at $x = 0.5$ in comparison with the theoretical diffraction pattern of $Rb_2Zn_3(P_2O_7)_2$ constructed from structural data [26].

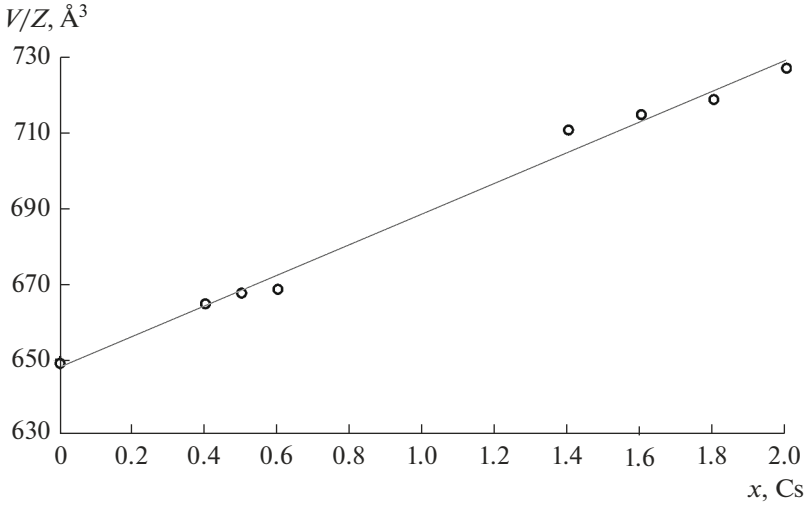

Fig. 3. Dependence of the crystallographic volume occupied by the formula unit on the content of cesium (the line shows the approximation).

mentioned above confirms the construction of the structure of the considered phases from the P_2O_7 dimers.

Complex thermal analysis was used to study the behavior of the obtained ceramic materials upon heating. Based on this study and information about the concentration boundaries of the existence of the detected solid solutions, a preliminary diagram of phase equilibria was built, shown in Fig. 5. The solidus and liquidus lines are shown as dotted lines due to the insufficient number of samples under consideration and will be refined in the future.

The results of DSC and thermogravimetry (TG) for samples corresponding to the region of crystallization of the noncentrosymmetric phase I are shown in Fig. 6. The melting temperature, determined by plotting the tangents to the DSC curve of both presented compositions, is 750–752°C. Based on the nature of the DSC curves, it can be concluded that the melting behavior of the putative $K_3CsZn_6(P_2O_7)_4$ compound is congruent with very similar solidus and liquidus temperatures in the region of the formation of a solid solution (phase I). This type of melting allows us to hope

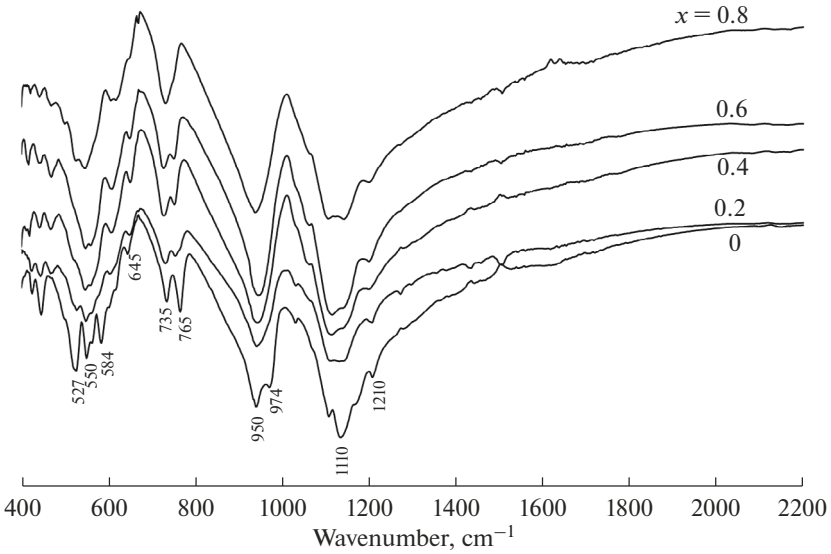

Fig. 4. IR spectra of synthesized samples at $0.0 \le x \le 0.8$.

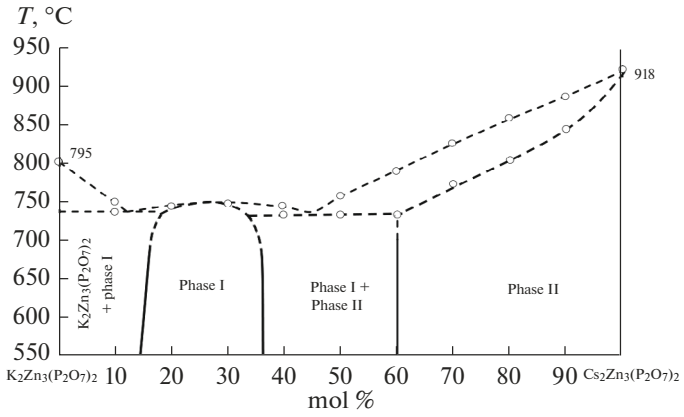

Fig. 5. Assumed diagram of phase equilibria of the studied system.

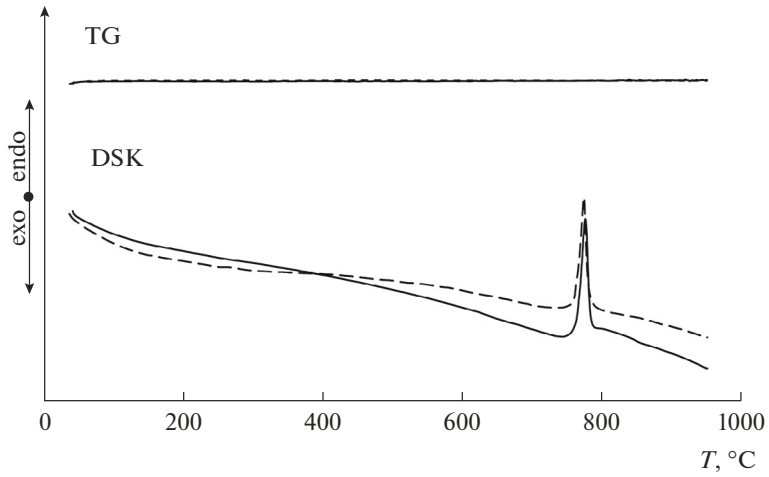

Fig. 6. Results of complex thermal analysis of samples of $K_{2-x}Cs_xZn_3(P_2O_7)_2$ composition at $x = 0.4$, solid line; and $x = 0.6$, dotted line (phase I).

for the possibility of growing single crystals of this compound by crystallization from a melt.

CONCLUSIONS

A new zinc phosphate crystallizing in the space group $P2_1$ was found in the concentration range of $0.4 \le x \le 0.6$ of the $K_{2-x}Cs_xZn_3(P_2O_7)_2$ compositions (phase I). By analogy with isostructural zinc phosphates, this phase can be expected to have nonlinear optical properties together with high transparency in the ultraviolet range. The formation of a solid solution at $1.4 \le x \le 2.0$ based on the $Cs_2Zn_3(P_2O_7)_2$ compound (phase II) is confirmed.

FUNDING

This study was carried out as part of a state task of Grebenshchikov Institute of Silicate Chemistry, Russian Academy of Sciences (subject no. 0081-2022-0008).

CONFLICT OF INTEREST

The authors of this work declare that they have no conflicts of interest.

REFERENCES

1. Volkov, S., Petrova, M., Sinel'shchikova, O., Firsova, V., Popova, V., Ugolkov, V., Krzhizhanovskaya, M., and Bubnova, R., Crystal structure and thermal properties of the $Li_xNa_{1-x}KZnP_2O_7$ solid solutions and its relation to the $MM'ZnP_2O_7$ diphosphate family, *J. Solid State Chem.*, 2019, vol. 269, pp. 486–493.
2. Sunitha, A.M., Gopalakrishna, G.S., and Byrappa, K., Comparative study of impedance properties of $LiHZn(P_2O_7)$, $Na_2ZnP_2O_7$–HCl and $KHZnP_2O_7$ crystals, *J. Int. Acad. Res. Multidiscipl.*, 2016, vol. 4, no. 2, pp. 329–339.
3. Voronin, V.I., Sherstobitova, E.A., Blatov, V.A., and Shekhtman, G.Sh., Lithium-cation conductivity and crystal structure of lithium diphosphate, *J. Solid State Chem.*, 2014, vol. 211, p. 170.
4. Saha, S., Rousse, G., Fauth, F., Pomjakushin, V., and Tarascon, J.-M., Influence of temperature-driven polymorphism and disorder on ionic conductivity in $Li_6Zn(P_2O_7)_2$, *Inorg. Chem.*, 2019, vol. 58, no. 3, p. 1774.
5. Kharroubi, M., Assad, H., Gacem, L., and Henn, F., Study of dielectric relaxation phenomena of $Na_2ZnP_2O_7$ diphosphate glass dopped with cobalt(II) by impedance spectroscopy, *Int. J. Emerg. Technol. Adv. Eng.*, 2014, vol. 4, no. 7, p. 49.
6. Averbuch-Pouchot, M.T., Crystal data on $Zn_3Rb_2(P_2O_7)_2$ and $Co_3Rb_2(P_2O_7)_2$. Crystal structure of $Zn_3Rb_2(P_2O_7)_2$, *Zeitschr. Kristallogr.*, 1985, vol. 171, pp. 113–119.
7. Caldiño, U., Lira, A., Meza-Rocha, A.N., Camarillo, I., and Lozada-Morales, R., Development of sodium-zinc phosphate glasses doped with Dy^{3+}, Eu^{3+} and Dy^{3+}/Eu^{3+} for yellow laser medium, reddish-orange and white phosphor applications, *J. Lumin.*, 2018, vol. 194, p. 231.
8. Soriano-Romero, O., Lozada-Morales, R., Meza-Rocha, A.N., Carmona-Téllez, S., Caldino, U., Flores-Desirena, B., and Palomino-Merino, R., Cold bluish white and blue emissions in Cu^+-doped zinc phosphate glasses, *J. Lumin.*, 2020, vol. 217, p. 116791.
9. Shwetha, M. and Eraiah, B., Influence of Dy^{3+} ions on the physical, thermal, structural and optical properties of lithium zinc phosphate glasses, *J. Non-Cryst. Solids*, 2021, vol. 555, p. 120622.
10. Quinn, C.J., Beall, G.H., and Dickenson, J.E., Alkali zinc pyrophosphate glasses for polymer blends, *Bull. Span. Soc. Ceram. Class.*, 1992, vol. 4, p. 79.
11. Rivera, F.L.F., Velázquez, D.Y.M., Aldaya, I., and Pérez-Sánchez, G.G., Characterization of the optical gain in erbium–ytterbium–doped zinc and sodium–zinc phosphate glasses, *Opt. Mater. Express*, 2022, vol. 12, pp. 4491–4498.
12. Khelloufi, M., Kharroubi, M., Gacem, L., Balme, S., and Assad, H., Electrical conductivity and dielectric properties of rare earth ions (Ce^{3+}, Pr^{3+} and Eu^{3+}) doped in zinc sodium phosphate glass, *J. Non-Cryst. Solids*, 2021, vol. 567, p. 120933.
13. Rayan, D.A. and Elbashar, Y.H., Spectroscopic analysis of potassium zinc phosphate glass matrix doped CuO for optical filter applications, *J. Opt.*, 2020, vol. 49, pp. 564–572.
14. Langar, A., Bouzidi, Ch., Elhouichet, H., and Férid, M., Er-Yb codoped phosphate glasses with improved gain characteristics for an efficient 1.55 μm broadband optical amplifiers, *J. Lumin.*, 2014, vol. 148, pp. 249–255.
15. Liu, Q., Dang, P., Zhang, G., Lian, H., Li, G., Molokeev, M.S., Cheng, Z., and Lin, J., Broad luminescence tuning in Mn^{2+}-doped $Rb_2Zn_3(P_2O_7)_2$ via doping level control based on multiple synergies, *CrystEngComm*, 2022, vol. 24, pp. 5622–5629.
16. Zhu, Sh.-Y., Zhao, D., and Liu, W., A broad emission band of phosphor $Cs_2Zn_3(P_2O_7)_2:Mn^{2+}$ induced by multi-sites of Mn^{2+}, *Inorg. Chem. Comm.*, 2023, vol. 150, p. 110397.
17. Rim, B., Lakhdar, G., Bachir, B., Hassan, A.A., Mohamed Toufik, S., Boubakeur, S., Elhadj Ahmed, G., Ahmed, G., and Guerbous, L., Synthesis and luminescence spectroscopy study of a novel orange-red (OR) color emissions phosphor based on Tb^{3+} ion doped $Na_2ZnP_2O_7$, *Luminescence*, 2021, vol. 36, no. 2, p. 489.
18. Bhake, A.M., Parauha, Y.R., and Dhoble, S.J., Synthesis and photoluminescence study of Ce^{3+} ion-activated $Na_2ZnP_2O_7$ and $Na_4P_2O_7$ pyrophosphate phosphors, *J. Mater. Sci., Mater. Electron.*, 2020, vol. 31, p. 548.
19. Guerbous, L. and Gacem, L., Synthesis and luminescent properties of Eu^{3+} doped crystalline diphosphate $Na_2ZnP_2O_7$, *Acta Phys. Polon. A*, 2012, vol. 122, no. 3, p. 535.
20. Amara, A., Gacem, L., Gueddim, A., Belbal, R., Soltani, M.T., and Guerbous, L., Luminescence properties of Cr^{3+} ions in $Na_2ZnP_2O_7$ crystal, *Phys. B* (Amsterdam), 2018, vol. 545, p. 408.

21. Fhoula, M. and Dammak, M., Optical spectroscopy of thermal stable $Na_2ZnP_2O_7:Sm^{3+}/(Li^+, K^+)$ phosphors, *J. Lumin.*, 2019, vol. 210, p. 1.

22. Belbal, R., Gacem, L., and Bentria, B., Blue emission of Co^{2+} in $K_2ZnP_2O_7$ phosphors, *Inorg. Chem. Commun.*, 2018, vol. 97, p. 39.

23. Zhao, S.G., Yang, X.Y., Yang, Y., Kuang, X.J., Lu, F.Q., Shan, P., Sun, Z.H., Lin, Z.S., Hong, M.C., and Luo, J.H., Noncentrosymmetric $RbNaMgP_2O_7$ with unprecedented thermo-induced enhancement of second harmonic generation, *J. Am. Chem. Soc.*, 2018, vol. 140, pp. 1592–1595.

24. Zhao, S.G., Gong, P.F., Luo, S.Y., Bai, L., Lin, Z.S., Ji, C.M., Chen, T.L., Hong, M.C., and Luo, J.H., Deep-ultraviolet transparent phosphates $RbBa_2(PO_3)_5$ and $Rb_2Ba_3(P_2O_7)_2$ show nonlinear optical activity from condensation of $[PO_4]^{3-}$ units, *J. Am. Chem. Soc.*, 2014, vol. 136, pp. 8560–8563.

25. Wu, H., Liu, S., Cheng, S., Yu, H., Hu, Zh., Wang, J., and Wu, Y., Syntheses, characterization, and theoretical calculation of $Rb_2Mg_3(P_2O_7)_2$ polymorphs with deep-ultraviolet cutoff edges, *Sci. China Mater.*, 2020, vol. 63, pp. 593–601.

26. Song, Z., Yu, H., Wu, H., Hu, Z., Wang, J., and Wu, Y., Syntheses, structures and characterization of non-centrosymmetric $Rb_2Zn_3(P_2O_7)_2$ and centrosymmetric $Cs_2M_3(P_2O_7)_2$ (M = Zn, Mg), *Inorg. Chem. Front.*, 2020, vol. 7, pp. 3482–3490.

27. Yu, H., Young, J., Wu, H., Zhang, W., Rondinelli, J.M., and Halasyamani, P.Sh., $M_4Mg_4(P_2O_7)_3$ (M = K, Rb): Structural engineering of pyrophosphates for nonlinear optical applications, *Chem. Mater.*, 2017, vol. 29, p. 1845.

28. Srivastava, A.M., Comanzo, H.A., Camardello, S., Chanry, S.B., Aycibin, M., and Happek, U., Unusual luminescence of octahedrally coordinated divalent europium ion in $Cs_2M^{2+}P_2O_7$ (M^{2+} = Ca, Sr), *J. Lumin.*, 2009, vol. 129, pp. 919–925.

29. Lapshin, A.E. and Petrova, M.A., Synthesis and crystal structure of the low-temperature modification of lithium potassium zinc diphosphate $LiKZnP_2O_7$, *Glass. Phys. Chem.*, 2009, vol. 35, pp. 637–642.

30. Petrova, M.A. and Sinel'shchikova, O.Yu., Triangulation in the $Li_2ZnP_2O_7$–$Na_2ZnP_2O_7$–$K_2ZnP_2O_7$ system, *Russ. J. Inorg. Chem.*, 2022, vol. 67, no. 2, pp. 209–215.

31. Song, H., Zhang, Sh., Li, Y., Liu, W., Lin, Z., Yao, J., and Zhang, G., Syntheses, crystal structures, and characterizations of three new pyrophosphates $CsNaZnP_2O_7$, $RbNaZnP_2O_7$, and $RbLiMgP_2O_7$, *Solid State Sci.*, 2019, vol. 95, p. 105940.

32. Ji, L.N., Cai, G.M., Li, J.B., Luo, J., Liang, J.K., Zhang, J.Y., Liu, Y.H., Rao, G.H., and Chen, X.L., Crystal structure and thermal properties of compound $K_2Zn_3(P_2O_7)_2$, *Powder Diffract.*, 2008, vol. 23, no. 4, pp. 317–322.